

Deep Learning for Multiwell Automatic Log Correction¹

Vanessa Simoes², Hiren Maniar², Aria Abubakar², and Tao Zhao²

ABSTRACT

Researchers have dedicated numerous applications of machine-learning (ML) techniques for field-scale automated interpretation of well-log data. A critical prerequisite for automatic log processing is to ensure that the log characteristics are reasonably consistent across multiple wells. Manually correcting logs for consistency is laborious, subjective, and error prone. For some wellbore logs, such as gamma ray and neutron porosity, borehole effects and miscalibration can cause systematic inconsistencies or errors that might be present even after the application of wellbore and environmental corrections.

Biased or consistently inaccurate data in the logs can confound ML approaches into learning erroneous relationships, leading to misinterpretations, such as wrong lithology prediction, reservoir estimation, and incorrect formation markers.

To overcome such difficulties, we have developed a deep learning method to provide petrophysicists with a set of consistent logs through the multiwell automatic log correction (MALC) workflow. Presently, the corrections we target are systematic errors on the standard logs, especially gamma ray and neutron logs, random noises, and to a lesser extent, local formation property misreading due to washouts.

We applied the proposed method in multiple fields worldwide containing different challenges, and in this paper, we include the results in two field examples. The first one covers the correction of synthetic coherent noise added to field data, and the second example covers the correction applied to original measurements.

INTRODUCTION

Traditionally, as part of the wellbore-log preprocessing step, petrophysicists may perform manual log normalizations using histograms and crossplots (Neinast and Charles, 1973; Aly et al., 1997; Xu et al., 2016), reference values for certain formation types, such as pure calcite, anhydrite, and shale (Shier, 2004), percentile-based normalizations (Quartero et al., 2014), or the use of synthetic generated logs (Xu et al., 2016). The reference formation types approach is time consuming and requires the presence and identification of reference lithologies and corrections that do not consider any form of zonation present risks described in Appendix 1. Moreover, those proposed methods lack a systematic way to quantify uncertainty.

MALC is a new workflow that uses deep learning to contextually correct logs as per the relevant regional references discovered and learned during the ML training. An approach similar to an unsupervised denoising ML is employed to enable this procedure, using a customized set of noises and artifacts to corrupt and correct the input

samples. We train the ML method to discover regional/contextual references, and it learns to apply the correction accordingly. The proposed method does not predefine fixed rules to the log correction but allows the ML model to learn from representative samples. Therefore, it is flexible and adaptive compared to traditional methods, and the ML learns to perform multiple alterations simultaneously. Another advantage is that MALC provides an uncertainty interval for the corrected log. One current limitation over other methods is requiring multiple reference wells for train and validation.

Our current work focuses on a correction for neutron and gamma ray logs that require modifications with higher probability and relative intensity than other logs. We will pursue other measurements afflicted by systematic or random errors in the future. Extension to new applications should be feasible if common disturbances affecting the wellbore-log measurements are well understood and modeled.

The improvement provided by this technique relies on the ability of deep learning to understand the context, learn the expected type of correction required, and perform the

Manuscript received by the Editor August 1, 2022; revised manuscript received October 28, 2022; manuscript accepted October 31, 2022.

¹Originally presented at the SPWLA 63rd Annual Logging Symposium, Stavanger, Norway, June 11–15, 2022, Paper 0070.

²SLB, vsimoes@slb.com; hmaniar@slb.com; abubakar@slb.com; tzha03@slb.com

relevant log alterations. For the end user, there is no need to explore and identify reference lithologies in the well or field. Once trained, the model can be quickly applied to nearby wells with lesser expert supervision, provided triple-combo or quad-combo logs are available. Finally, the proposed methodology results in a faster turnover time than traditional approaches.

The log correction performed in the MALC workflow is an essential step to improve data consistency in log quality control. Data consistency is one of the most important dimensions in data quality, and it “specifies that two data values drawn from separate data sets must not conflict with each other.” Moreover, it does not imply correctness (Loshin, 2008). For other steps to improve wellbore-log data quality, please see McDonald (2021) and Simoes et al. (2022). In our current log quality control approach, MALC is being applied after the intervals with non-natural signals have been adequately identified (intervals filled with straight lines and outside an interval of accepted values), as in Fig. 1.

Our results can contribute to improving multiple downstream applications, such as shear prediction (Anemangely et al., 2019), lithology prediction (Chen et al., 2020a), porosity estimation (Chen et al., 2020b), and formation markers (Abubakar et al., 2021).

We appreciate the risks involved in correcting logs, especially in a fully automated mode. The current methodology provides the expert with a tool that can be deployed together with an expert review and acceptance of results. Part of the risks are derived from the different formation properties’ effect on different curves, such as low sensitivity to fluid properties on gamma ray when compared

to other logs or higher sensitivity of gamma ray to radioactive properties possibly heterogeneously distributed along the field. While using multiple logs increases the possibility of separation between errors and alterations in formation properties, the risk is still present.

This work provides more technical details regarding the methodology and two field studies—one field application for synthetic noises and one for original field noise. The applications provide an increasing difficulty level, from fixed shift and multiplication factor on a gamma ray log to concluding with varying alterations in multiple log types.

STUDY CONSIDERATIONS

The development of this work is motivated by our use of window-based ML methods to predict missing logs in the challenging scenarios of multiple missing wellbore-log types in the original data set and our success in detecting zones or wells where the predicted logs had a shift relative to the original data.

This method has been developed and tested on several oil fields worldwide, demonstrating reliable results on logs with both cases, synthetically induced errors and original systematic errors.

We successfully conducted field tests in two scenarios. The first scenario was to correct for systematic errors in the gamma ray logs when other logs, such as resistivity, density, and neutron porosity, are available. The second scenario is to identify and correct both systematic and local errors in gamma ray and neutron porosity logs when gamma ray, neutron porosity, density, and resistivity logs are available.

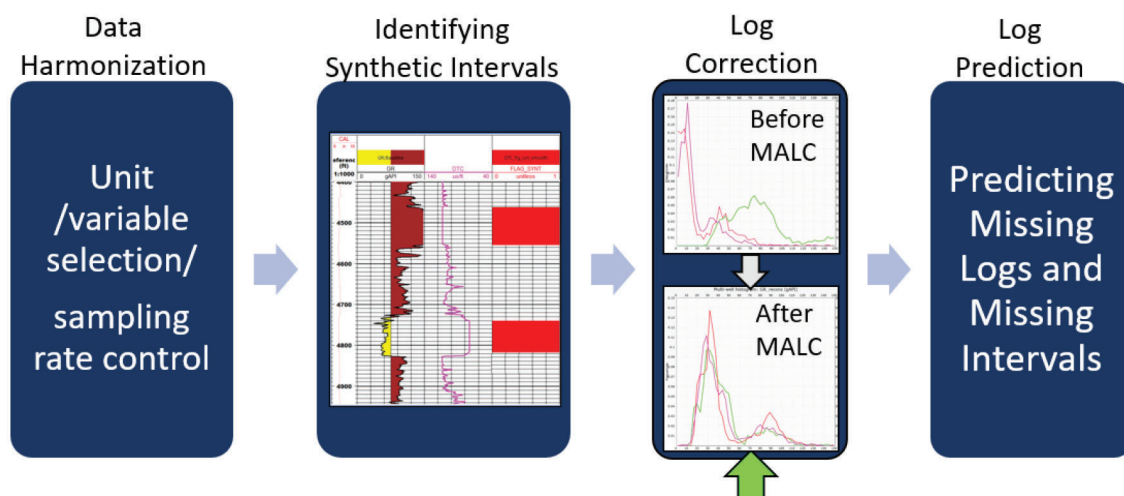


Fig. 1—General log quality control steps to build a high-quality wellbore-log data set, with the green arrow indicating the log correction step performed by MALC workflow.

To some extent, the method also accounts for local errors in density and neutron porosity logs; those errors may occur in zones where the pads may face problems maintaining contact with the formation. A case of correction of synthetic alteration to the density log is included in this study.

We test our approach using two public data sets with different availability of logs, each with unique challenges. The Bakken data set consists of a subset of wells with good-quality logs and no predominant shift. For this reason, we use this data set to evaluate the ML model in the synthetically induced errors in the wellbore logs.

The second data set is from the Groningen Field in the northeastern Netherlands. This data set contains wells with intense shifts in the gamma ray and neutron porosity logs. We employ this data to demonstrate the log correction performance in wellbore logs with original systematic errors.

MALC workflow is described in Fig. 2, which contains the steps to build the deep learning model to perform the correction and the final application of this method to selected wells presenting high dissimilarity. As a result of this workflow, MALC improves the consistencies between logs from a field containing multiple wells, for example, when reinterpreting a mature field and evaluating an open database or when aiming for consistent corrections between logs acquired using multiple tool specifications.

These inconsistencies can happen even after borehole and environmental corrections have been applied. The reinterpretation of large data sets with limited information on tool specifications, drilling fluid properties, possible problems with mud circulation, and changes in drilling fluid along the survey is becoming more frequent with the digitalization of the industry.

Experts performing log analysis on multiple wells in the same field would apply this method as a preprocessing step before performing volume of shale and porosity computation, marker detection, or seismic wellbore-log integration. MALC is of particular interest when (a) reinterpreting a mature field with tens or hundreds of wells with triple combo only, (b) when there are a few corrected logs by an expert and the extrapolation for other wells is required, or (c) when there is a signal which is not reflecting the formation, and it is required to attenuate the influence of noise.

METHODOLOGY

To build a ML model using the data noted above, we first need to identify a set of high-quality wells with logs exhibiting weak systematic errors. These wells will be used as training and validation data to optimize the neural network weights and further evaluate how well the trained model can perform the tasks.

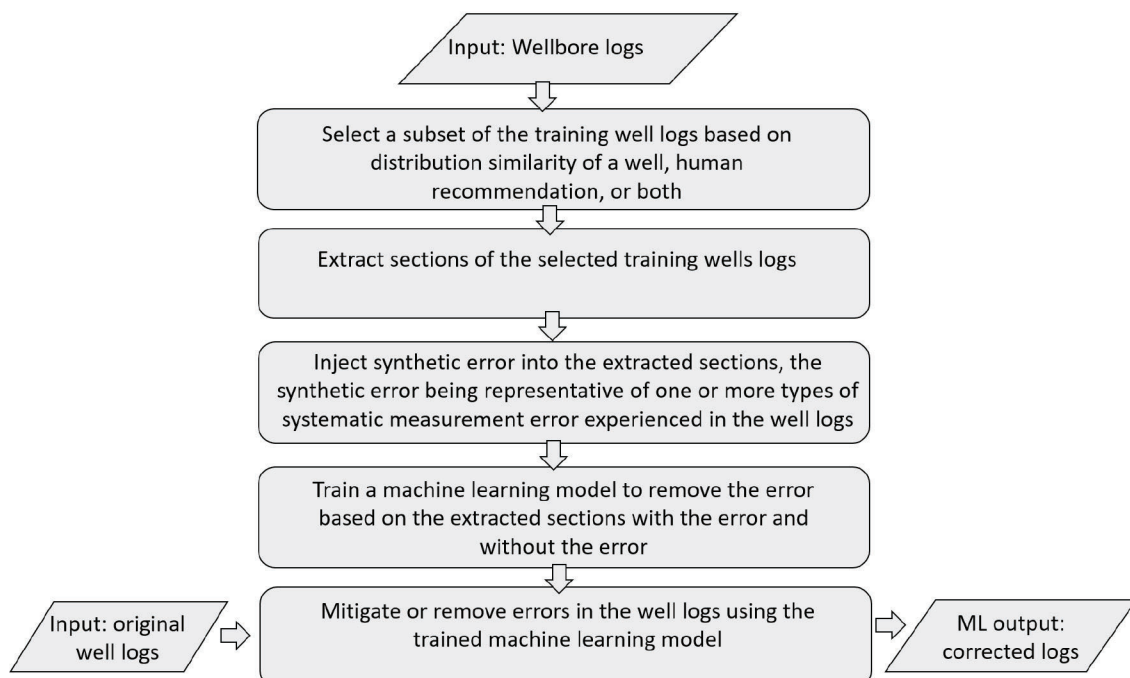


Fig. 2—Workflow for MALC application on a field.

In addition to performing quality control during the selection of training wells, ensuring sufficient diverse representation and inclusion of multiple formation types encountered in the test wells is essential.

The first step is a selection of high-quality training and validation wells conducted in a semiautomatic fashion. A statistical methodology is adopted to identify logs with similar distributions. To quantify dissimilarity among the wellbore logs from different wells, we use a quantity based on relative entropy or Kullback-Leibler (KL) divergence (Gibbs and Su, 2002). In addition to this statistical selection based on distribution similarity, one could also select wells based on expert recommendations or use wells that experts already corrected. This step aims to establish reference wells (identified as type wells in Neinast and Charles (1973) and Shier (2004)) on which the ML model can correctly learn the actual log behavior. Such reference wells should reflect the expected correction and contain various formation types that sufficiently represent the subsurface condition.

In the first step, we use KL divergence (Eq. 1) as a base to compute the dissimilarity (D) (Eq. 2) between two distributions of the same log from different wells. Ideally, this evaluation should be used for the same zonation or wells with proportionately similar formation types; in the two examples presented in this paper, the dissimilarity is shown for intervals containing similar mineralogy.

$$KL(p, q) = \sum_{x=1}^n p(x) \ln \left(\frac{p(x)}{q(x)} \right). \quad (1)$$

$$D(p, q)^2 = (KL(p, r) + KL(q, r)). \quad (2)$$

Here, KL represents the KL divergence, p and q are discretized distributions associated with a log of interest in two different wells and $r = (p + q)/2$, and n is the number of subintervals used in the discretization.

The measure in dissimilarity (D) provides a symmetric quantity (Endres and Schindelin, 2003) that represents a concise way to identify wells that have similar distributions along an interval of interest and wells that are dissimilar to each other concerning a particular log. This measure also helps to access the results when applying MALC to the test wells to field data with original noise where the ground truth curves are not available for a quantitative analysis based on mean absolute error (MAE), mean square error (MSE), root mean square error (RMSE), or PSNR (peak signal-to-noise ratio, or a logarithmic representation of MSE) would not be possible. To evaluate the method using validation wells or, in general, when the logs present negligible alterations, we use quantitative metrics, such as MAE, MSE, MSE_90, MAE_90, Pearson correlation coefficient, and PSNR. To

reduce the impact of outliers when presenting the results, we used MSE_90 and MAE_90, which represent the mean square error and the mean absolute error of the entire well after we disregarded the worst 10 percentile depths that presented the largest error. For the Pearson correlation coefficient, all points are included. For the PSNR calculation, we maintain consistency with the metrics indicated in the tables. The best 90% of the points (MSE_90) are used for the Bakken examples, and all points (MSE) are used for the Groningen example.

To illustrate those quantities with the distribution of the log, we presented the dissimilarity matrix and the multiple metrics for evaluation for a subset of wells from the two field case studies presented in this work in different scenarios and levels of noise.

The second step is the core process of this workflow. It takes samples of random intervals from multiple logs in the training wells to train a one-dimensional (1D) ML method to identify and correct systematic errors, such as shifts, differences in scaling factors, random noises, and minor local disturbances. The ML method used for this correction has a similar architecture compared to the window-based convolutional neural network autoencoder (WAE) method presented in (Simoes et al., 2022), which comprises a convolutional neural network (CNN) method with an architecture similar to the U-Net (Ronneberger et al., 2015) adapted for a 1D problem, as illustrated in Fig. 3, and the model is trained using a self-supervised strategy.

We selected a window-based approach using a CNN as this window-based ML method was selected over other alternatives because it indicated the ability to capture logs intercorrelation and depth-sequence correlation. Other window-based methods can be explored in future architectures.

The input layer contains all logs of interest in the model, and the encoder and decoder blocks contain the subsequent hidden layers. The first half of the architecture holds the encoder blocks with 1D convolutional layers using rectified linear unit (ReLU) activation functions and 1D max pooling layers to downsample the inputs by taking the maximum value of the convolutional span.

The second half of the model contains the decoder blocks with 1D convolutional layers and up-sampling layers to recompose the dimension reduced using the max pooling in the encoder blocks.

The model also has skip connections linking the encoder and decoder blocks to enable the model to capture the data behavior at multiple scales. The impact of those layers accelerated the convergence and improved the data reconstruction for higher-frequency modes.

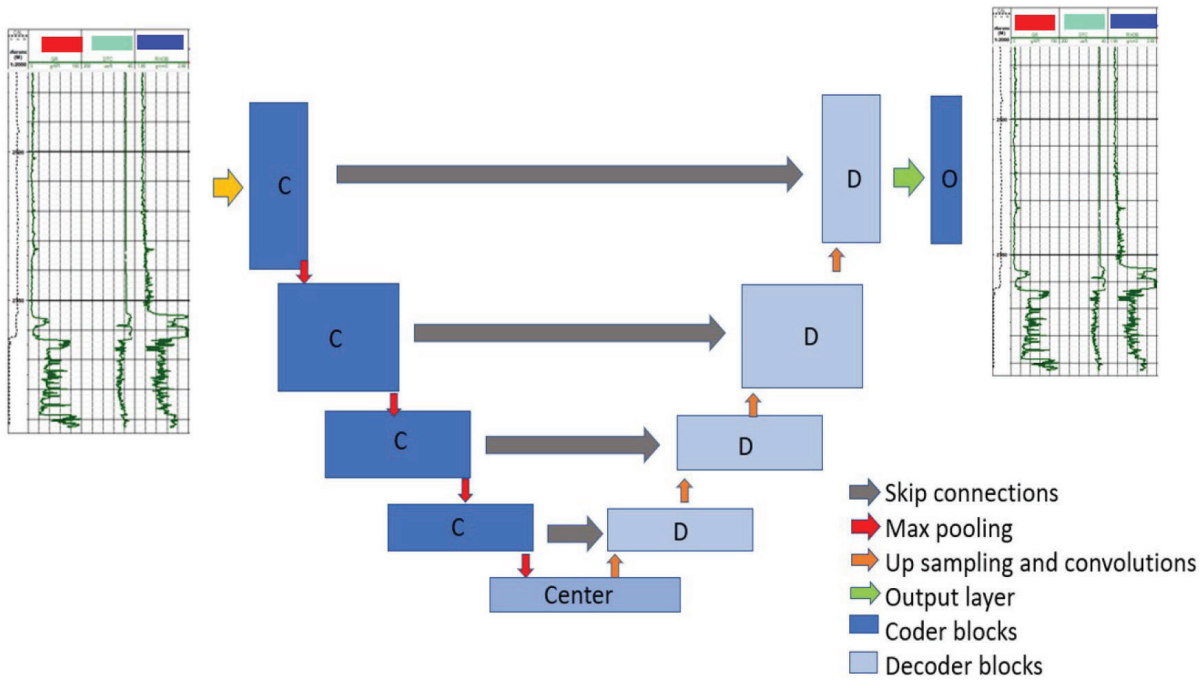


Fig. 3—Scheme for the proposed deep learning method used to perform the log correction. The left side shows the input intervals containing altered samples using a combination of randomly applied distortions, the middle part includes the deep learning method, and the right side has the denoised intervals.

The objective function being minimized is the MAE or the MSE between the original and the ML-corrected samples. For model-weighting optimization, we use the Adam optimizer (Kingman and Ba, 2015) with a learning rate equal to 0.001 to minimize the loss function MAE or MSE. Moreover, we apply early stopping as an additional means of regularization or to terminate the training and reduce the overfitting impact. It is important to emphasize that dissimilarity or zonation is used for assessing the results but is not used while optimizing the ML model.

The adopted training paradigm is a critical difference between the method in Simoës et al. (2022) and the MALC method. While training the ML method for log correction, we performed input sample distortions using shifts and scaling with varying intensity and some local and minor random alterations, as indicated in Fig. 4.

The method adopted uses convolutional layers, allowing for varying sample sizes. The sample sizes used during training and validation in the examples provided in this paper are nearly 130 ft long. With this window size, capturing large-scale formation properties variation is possible. The entire

well is used as one sample during the inference stage. The fact that we use CNN layers in the method allows a change in input dimension. We tested multiple configurations for the CNN architecture and hyperparameters, but we have yet to exhaust the space to explore because of the multiple possible combinations.

While investigating multiple algorithms for log prediction (see Simoës et al., 2022), we compared multiple methods. The application in field data sets indicated that while multiple methods had the required properties in high-quality data sets, CNN-based methods maintained good-quality prediction, even in noisy data sets and data sets with multiple missing intervals. The contextual information also impacted the uncertainty band in a positive way, reducing the uncertainty interval when nearby points were available. Those other methods include random forest, XGBoost, and pointwise-based fully connected neural network layers. The proposed CNN method has the possibility of handling one or more missing logs, getting contextual information, and reducing ambiguity when multiple logs are impacted by alteration.

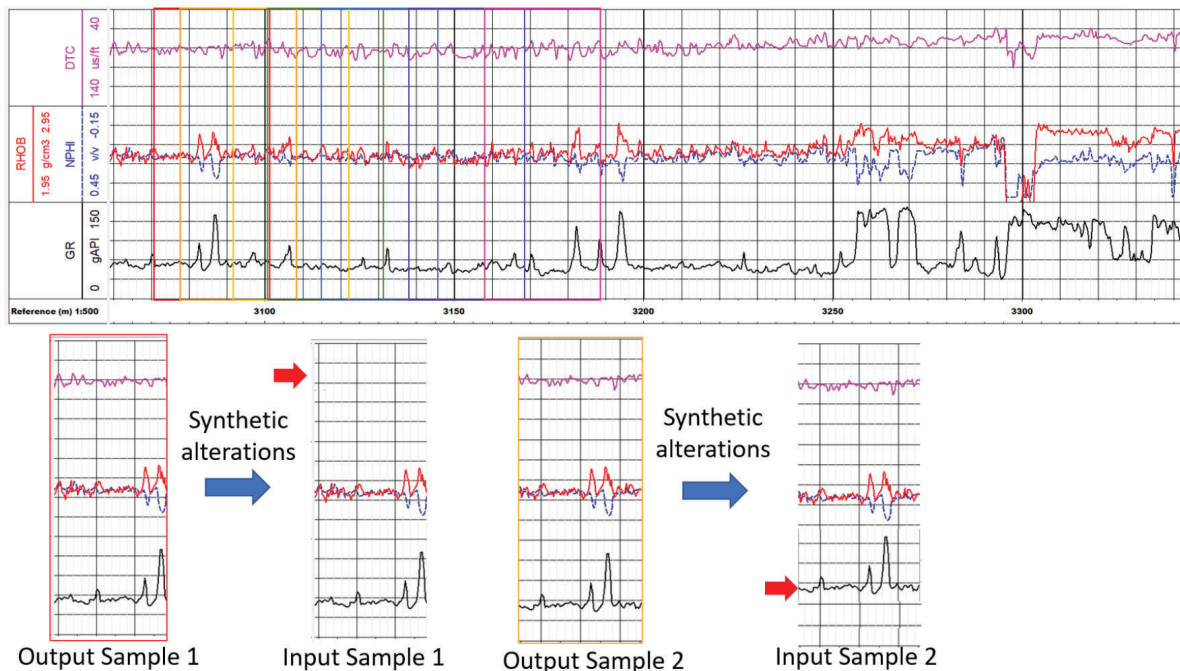


Fig. 4—Strategy for generating samples from training and validation wells. We select window-based samples from the training and validation wells, and systematic and random noises are added to the input samples to train the deep learning model.

The training process is self-supervised, as indicated in Figs. 4 and 5, and does not require human labels. We implement self-supervised training by adding noise and artifacts to the input samples, like what we expect in field data, and the training process behaves as a denoising autoencoder. Currently, the following types of noise and artifacts are added during training: lateral shift for neutron and gamma ray logs, differences in scaling factor for gamma ray logs, slight vertical shift for all wellbore logs, random noise for all logs, and local disturbances on density and neutron porosity logs. The authors are improving the training strategy to correct for local disturbances. A separate set of validation wells are used to evaluate the network performance. We monitor the validation error and use early stopping to avoid overfitting and, in turn, expect the model can generalize to unseen data.

Once the model is trained, it can be applied to other wells in the same formation. The output from the trained model contains the corrected log curves, a depth-by-depth standard deviation among the multiple realizations, and the uncertainty interval assuming a normal distribution among the multiple realizations.

To calculate the uncertainty for the corrected logs, we use the Monte Carlo Dropout technique, as proposed

by Gal and Ghahramani (2016). To account for the model uncertainty, we maintain the dropout layers activated in the neural network during the inference stage while also adding small random alterations to the input logs when calculating the inference multiple times. We save the average and the 10 and 90 percentiles from the numerous realizations. These percentiles provide an uncertainty band around the average value, which varies with depth, and can help identify zones or wells with higher uncertainty to be further manually reviewed by an expert. We have tested the hypothesis that for most depths in scenarios when all logs are available; the distribution provided from the multiple realizations follows a normal distribution.

CASE STUDIES

We successfully tested MALC in multiple field data, and it provided consistent results for gamma ray and neutron porosity corrections in different scenarios. This work contains the ML correction results progressing with the difficulty level.

The first application is performed on the Bakken Formation with field data, and synthetic noise is added to the wellbore logs, firstly to the gamma ray log only and secondly

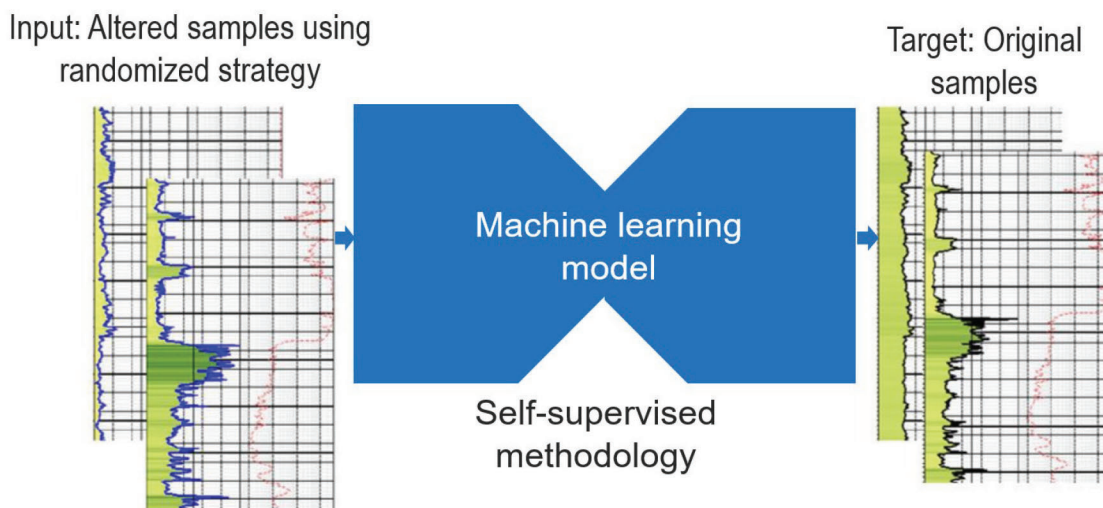


Fig. 5—Scheme for the self-supervised strategy used for training deep learning method to denoise logs from multiple sources of alterations.

to the gamma ray and neutron porosity simultaneously. In this case, the alterations added contain constant shifts and scaling factors over the entire well.

The second application is performed on the original Groningen Field data. In this case study, some log types presented alterations along the well that the ML model consistently corrected. The first results refer to the correction in reference layers formed by halite and anhydrite, and the last results refer to the reservoir.

Application on the Bakken Formation

This Bakken data set consists of 21 wells with triple-combo logs. The estimated porosity in the logged intervals varies from 0 to 13%, the estimated clay volume varies from 0 to 40%, and the measured depth varies from 7,300 to 11,700 ft.

Compared to other data sets we have analyzed, this data set has high-quality data with no indication of a washout effect in the logs, no missing intervals or logs, and no apparent substantial depth shift. Given the high-quality data, we randomly split the wells for training and validation. The histogram in Fig. 6 shows the distribution of the gamma ray log from all wells in this data set. Some differences between the wells are evident, but there is no strong apparent substantial shift. The black lines represent the wells that will be used for training and validation, and the red, magenta, and green colors represent the three test wells to be synthetically altered and used as examples for the MALC application.

We first tested the ability of the ML model to predict the corrected gamma ray log using artificially altered gamma ray, neutron porosity, density, and logarithmic resistivity as input to the model.

To train the model, we created a set of 1D intervals to be used as input samples by the unidimensional convolutional neural network (1DCNN) model and set the target logs as gamma ray, neutron porosity, and density.

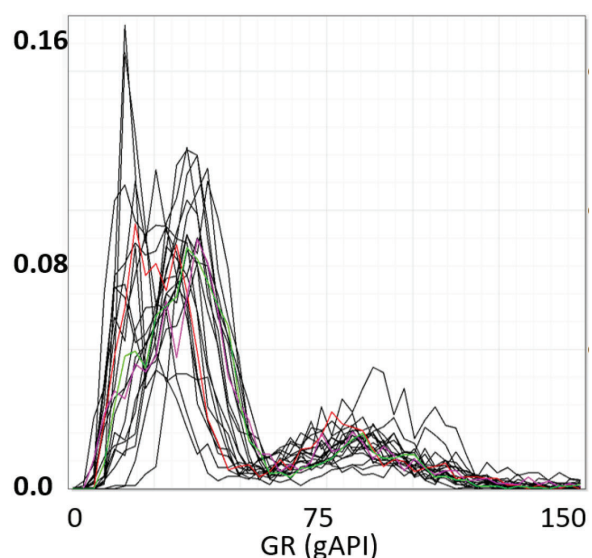


Fig. 6—Histogram for gamma ray log distribution in the original Bakken data set.

To test the log correction method on synthetic noise, we first added artificial noise to the gamma ray log only and compared the predicted gamma ray with the original data. Figure 7 shows the original logs' histogram in black and the distribution for three test wells containing synthetic noise. We plot Test Well A in green, Test Well B in magenta, and Test Well C in red.

It is possible to notice that the alteration applied to the original data has an intensity comparable to the signal. For the wellbore-log distribution in green from Test Well A, for example, the difference median between the altered and original gamma ray is 37 gAPI, while the median of the original gamma ray log is 35 gAPI.

In this application, by looking at the multiple GR distributions in Fig. 7, it is expected that the result from the ML method and a traditional quantile method for log normalization will provide similar results. The advantage of the proposed method over the quantile method is that the correction has local and not global behavior. It does not assume the distributions should be similar, allowing the method to be applicable to a subinterval of the field or a well without certain formations contributing to the overall distribution shape. Another advantage is the use of multiple logs as inputs allowing the identification of additional effects in the logs, such as caused by diagenesis, if similar behavior is present in the training wells.

The trained model using the training and validation wells was applied to the test wells with the corrupted/altering gamma ray logs. Furthermore, when looking at the gamma ray distribution, there was an improvement regarding the similarity with the original data set. Figure 8 contains the distribution before and after the correction.

Figure 9 contains a depth-by-depth depiction of a test well. The original log (red) and the ML-corrected logs (blue) are similar in terms of a general trend and intensity, even with the significant alteration added to the data (dark green).

It is possible to quantify the dissimilarity for the gamma ray log distribution using the dissimilarity measure, D , in the test wells. Table 1 contains the dissimilarity matrix for the original logs, Table 2 contains the dissimilarity matrix for the altered data (with artificial alteration), and Table 3 contains the dissimilarity matrix for the ML-corrected logs. The table has the information indicated in the histograms in Fig. 8 for the distributions before and after ML correction. Specifically, after adding synthetic noise, the dissimilarity between the curves increased for two of the three pairs of test wells. After the ML correction, the extent of distinction reaches a level similar to the original logs or smaller.

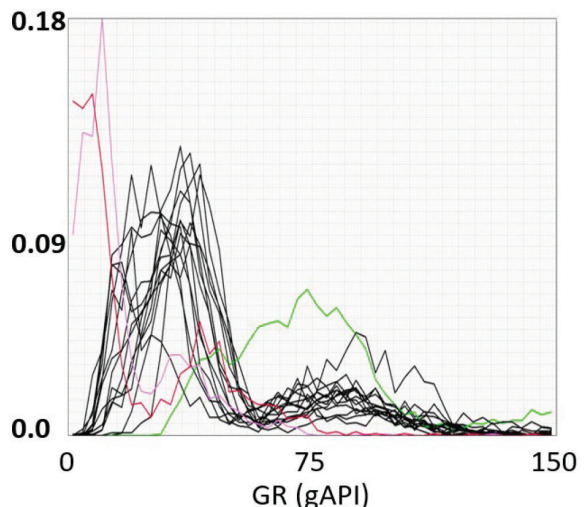


Fig. 7—Original gamma ray logs are plotted in black, while the test wells with synthetically noised added to the data are plotted in green, red, and magenta.

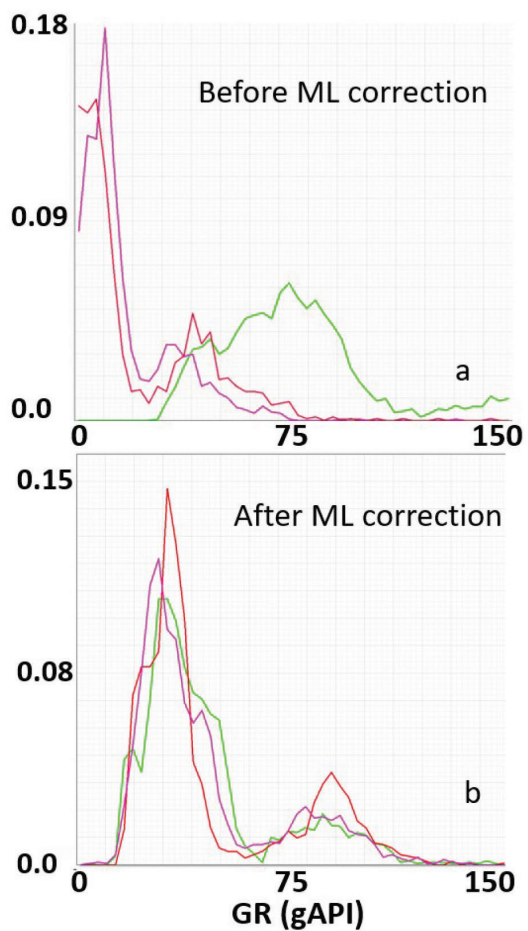


Fig. 8—Histogram for gamma ray distribution before and after applying the ML correction method. It is evident that after corrections, the distributions are more consistent with the other distributions seen in Fig. 6.

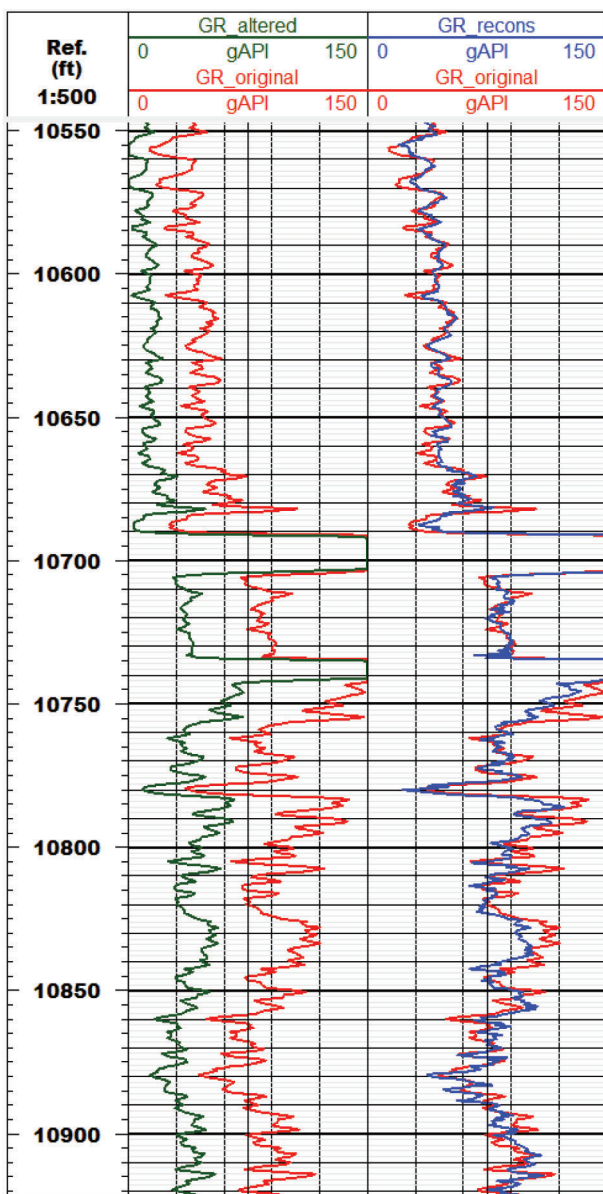


Fig. 9—Log plot for Test Well A showing the original gamma ray log in red, synthetically altered gamma ray log in dark green, and the ML-corrected curve in dark blue.

Table 1—Dissimilarity Matrix for the Original Gamma Ray Logs' Distribution for Three Test Wells

Before ML	Well A	Well B	Well C
Well A	0.00	0.16	0.32
Well B	0.16	0.00	0.31
Well C	0.32	0.31	0.00

Table 2—Dissimilarity Matrix for the Synthetically Altered Gamma Ray Logs' Distribution for Three Test Wells

Altered GR	Well A	Well B	Well C
Well A	0.00	0.37	0.47
Well B	0.37	0.00	0.24
Well C	0.47	0.24	0.00

Table 3—Dissimilarity Matrix for the MALC-Corrected Gamma Ray Logs' Distribution for Three Test Wells

After ML	Well A	Well B	Well C
Well A	0.00	0.17	0.29
Well B	0.17	0.00	0.22
Well C	0.29	0.22	0.00

The analysis using the dissimilarity (D) matrix, with each element calculated using Eqs. 1 and 2, helps to identify possible outliers in the original distribution and to understand the overall impact of the ML in reducing the dissimilarity.

When analyzing the dissimilarity, one needs to consider the different aspects that affect the distribution, such as the formation proportionality across the field, the diagenetic process altering the mineralogy in a heterogenous manner across the field, and even alterations in the resolution measurement vertical. The dissimilarity matrix represents the first indicator, and further analysis may help separate the dissimilarity cause.

A depth-by-depth depiction of a test well is presented in Fig. 9. The original log (red) and the ML-corrected wellbore logs (blue) are similar in terms of a general trend and intensity, even with the significant alteration added to the log (dark green).

The second test case performed in Bakken is the simultaneous alteration of neutron porosity and gamma ray curves. We used the same ML model when we altered only the gamma ray log or when we simultaneously added synthetic alterations to multiple logs. In this scenario, the crossplot in Fig. 10 contains the histogram for GR (a) and NPHI (d) and the scatter plot for NPHI vs. GR (b) and GR vs. NPHI (c). The train and validation wells (unaltered logs) are presented in black, and the test (synthetically altered wells) are presented in green (Well A), magenta (Well B), and red (Well C) and present a clear distinction when compared to the primary trend in black.

The level of noise varies between the wells, as indicated in Fig. 10 and Table 4. Well A has the lower-level noise, and Well C has the strongest noise in both GR and NPHI logs.

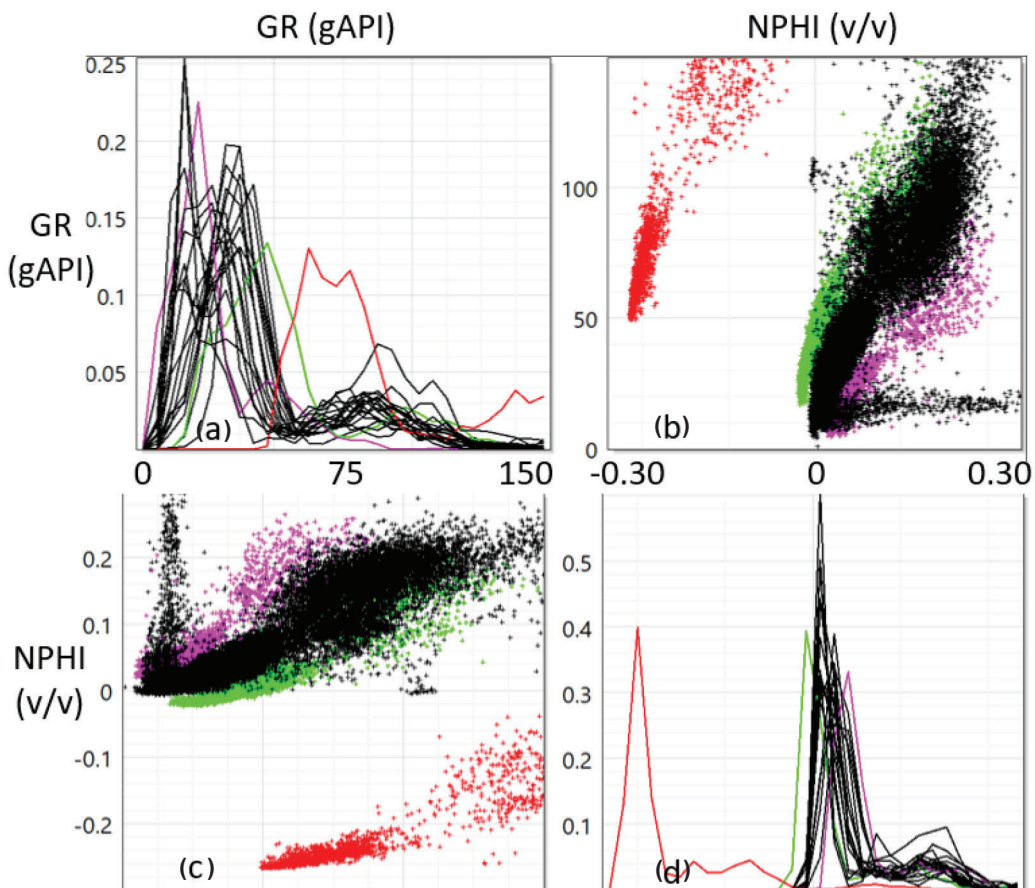


Fig. 10—Pair plot of GR and NPHI for train, validation, and test wells. Histograms of gamma ray (a) and neutron porosity (d) and scatter plots of gamma ray vs. neutron porosity (c) and neutron porosity vs. gamma ray (b). The test wells containing the original data plus an artificial alteration are plotted in green (Well A), magenta (Well B), and red (Well C), and the unaltered well logs are plotted in black.

During the inference stage, we added synthetic alteration simultaneously for both logs in the test wells, a scenario we incorporated into our training strategy. The log plot in Fig. 11 contains the results from such a test. The results show that the ML-corrected logs are closer to the original logs for gamma ray and neutron porosity and that the density log was not impacted during the correction. Additionally, comparing Tables 4 and 5, it is possible to notice that the MAE_90 and RMSE_90 reduced significantly for NPHI and GR for all

three wells and that RHOB continued close to the original log. It is also possible to notice that PSNR increased, and all those metrics indicate quantitatively that the signal quality improved.

The first track in Fig. 11 shows that the ML-corrected curve is smoother than the original log. For the Bakken data set, we only used 14 wells for training, which might have affected the capacity of the neural network to capture the high-frequency components.

Table 4—Metrics to Quantify the Level of Synthetic Noise Added to the Three Test Wells

Altered	Variable	MAE_90	RMSE_90	Pearson	PSNR
Well A	NPHI	0.02	0.02	1.00	28.62
Well A	GR	10.15	10.26	1.00	27.73
Well B	NPHI	0.02	0.02	1.00	27.91
Well B	GR	15.67	17.69	1.00	23.01
Well C	NPHI	0.27	0.27	1.00	6.91
Well C	GR	48.80	49.40	1.00	14.08

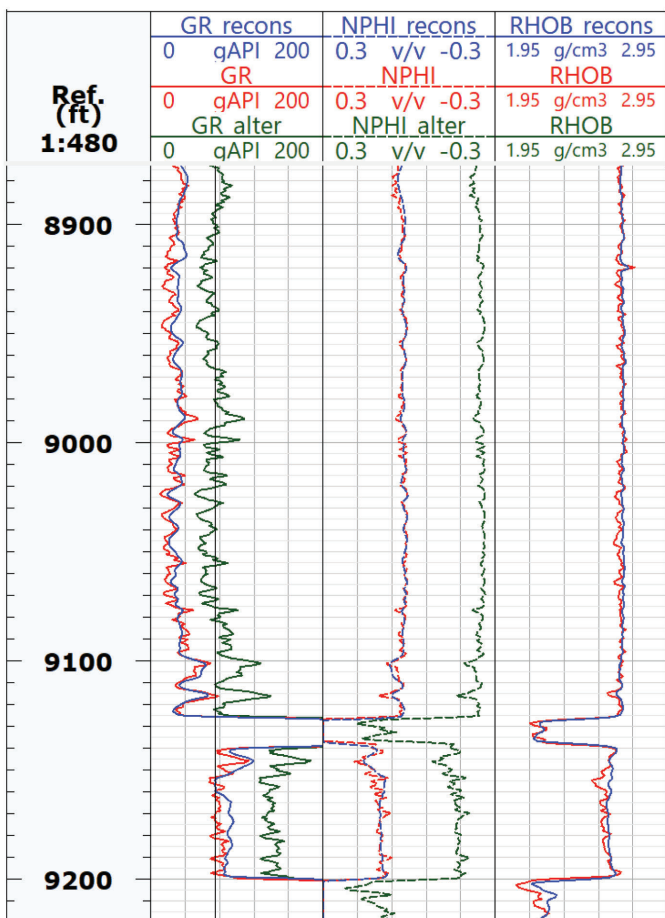


Fig. 11—Log plot depicting ML log correction for the Test Well C with simultaneous alterations in neutron and gamma ray logs. The original logs are in red, the altered logs are in green, and the ML-corrected logs are in dark blue. The first track shows the measured depths, the second track shows the gamma ray (GR), the third track shows the neutron porosity (NPHI), and the fourth track shows the density (RHOB).

Figure 11 and Table 5 indicate that applying MALC to the altered inputs reduced the distance from the original logs. This quantitative analysis using MAE_90, RMSE_90, Pearson correlation coefficient, and PSNR assumes that the ground truth is available and can be applied using validation wells presenting high-quality data.

These tests verify that the proposed ML methodology can provide log corrections in the presence of noise and artifacts. We conducted the tests using field data in two scenarios: alteration in the gamma ray log and simultaneous alteration in the gamma ray log and neutron porosity logs. In addition to the shifts and alterations to scaling factors applied to the original logs, the training strategy also accounted for random noises and, to a lesser degree, for local disturbances, and those targeted corrections guide the training strategy for the denoising autoencoder.

The last test performed using the Bakken field is applying MALC to the test wells without adding no synthetic alteration to the three test wells. As exemplified in Fig. 12, applying MALC did not cause any systematic shift or scaling in the gamma ray or neutron porosity logs, and it maintained the smoothing effect on the gamma ray present in the previous examples. Also, from the metrics presented in Table 6, the similarity between original and corrected RHOB and NPHI is very strong, and the Pearson correlation between ML-corrected and original gamma ray logs is also strong. Some differences are caused due to small depth shifts in the input and the smoothing effect.

Application on the Groningen Data Set

The second case study we consider is the Groningen Field (de Jager and Visser, 2017; Abubakar et al., 2022).

Table 5—Evaluation of the Logs Obtained Applying MALC to the Altered Logs

After MALC	Var	MAE_90	RMSE_90	Pearson	PSNR
Well A	NPHI	0.00	0.01	0.99	40.08
Well A	GR	3.56	4.36	0.97	35.17
Well A	RHOB	0.01	0.01	0.99	43.49
Well B	NPHI	0.01	0.01	0.99	39.49
Well B	GR	4.92	5.94	0.98	32.48
Well B	RHOB	0.01	0.01	0.98	41.72
Well C	NPHI	0.01	0.01	0.98	35.63
Well C	GR	6.96	8.28	0.96	29.60
Well C	RHOB	0.01	0.01	0.97	37.48

Table 6—Evaluation of the Logs Obtained Applying MALC to the Original Logs

After MALC	Var	MAE_90	RMSE_90	Pearson	PSNR
Well A	NPHI	0.00	0.00	0.99	42.42
Well A	GR	3.46	4.25	0.98	35.39
Well A	RHOB	0.01	0.01	0.99	43.92
Well B	NPHI	0.00	0.00	0.99	41.76
Well B	GR	4.74	5.70	0.97	32.84
Well B	RHOB	0.01	0.01	0.98	41.33
Well C	NPHI	0.00	0.01	0.99	39.55
Well C	GR	5.56	6.64	0.98	29.58
Well C	RHOB	0.01	0.01	0.99	31.51

We use a subset of 86 wells with the following logs: gamma ray, neutron porosity, density, compressional slowness, and resistivity.

This subset of logs from the Groningen Field represents an exciting data set with large sections of logged wells containing intervals with sandstones and shale and intervals with anhydrite and halite. Many of the wells present some systematic inconsistencies in the gamma ray and neutron porosity logs, as we will present shortly. To validate that the trained deep learning method using the self-supervised approach can provide good-quality corrected logs, we have performed a test similar to the application on the Bakken field, adding synthetic noise to the original logs for validation wells that present low dissimilarity to the test wells. Figure 13 presents the results for a sample from a validation well with low dissimilarity when the synthetic alteration is added simultaneously to gamma ray, neutron porosity, and density logs and the impact of applying MALC to this sample.

It is possible to notice in this plot that the MALC provided a better-quality log when compared to the original logs. As a result, MALC detects and corrects the synthetic alterations to this sample. The RMSE decreases, and the PSNR increases for that sample (see Table 7 and Table 8).

To evaluate the method using natural field noise in the Groningen data set, we focused on the layers containing anhydrite and halite, two minerals with a characteristic signature, with the pure mineral petrophysical properties shown in Table 9. Their presence allows us to detect the intervals with similar signatures. While the anhydrite presents an unusually high density and low compressional slowness, the halite presents a low density and very high resistivity. Many intervals formed predominantly by halite exhibit very low vertical variation in this field.

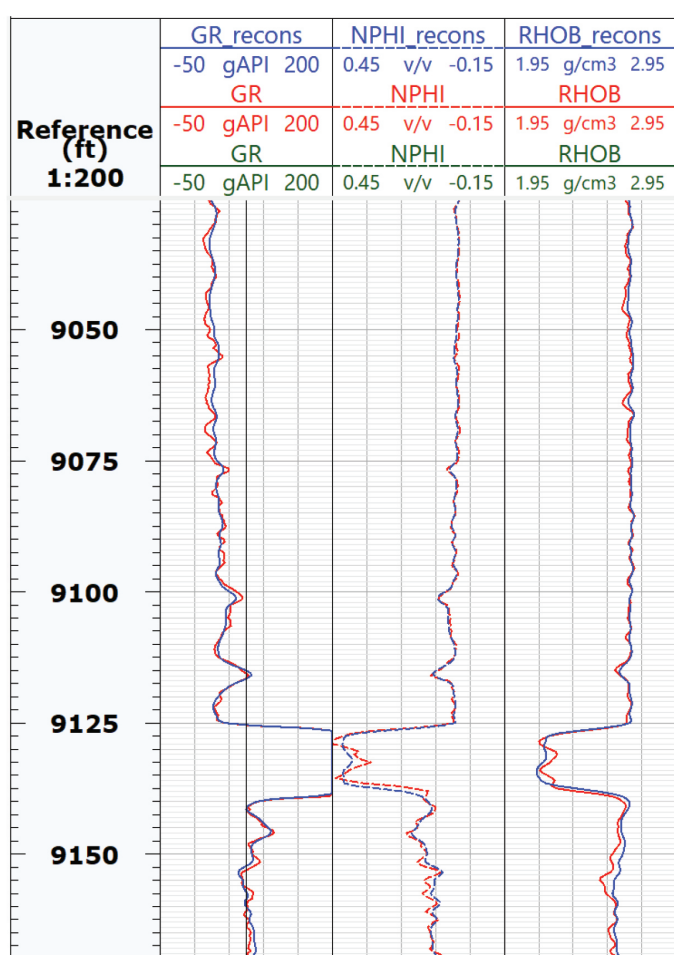


Fig. 12—Log plot depicting ML log correction for Test Well C. The first track shows the measured depths. The second track shows the gamma ray (GR). The third track shows the neutron porosity (NPHI), and the fourth track shows the density (RHOB). The original logs are in red, and the ML-corrected logs are in dark blue.

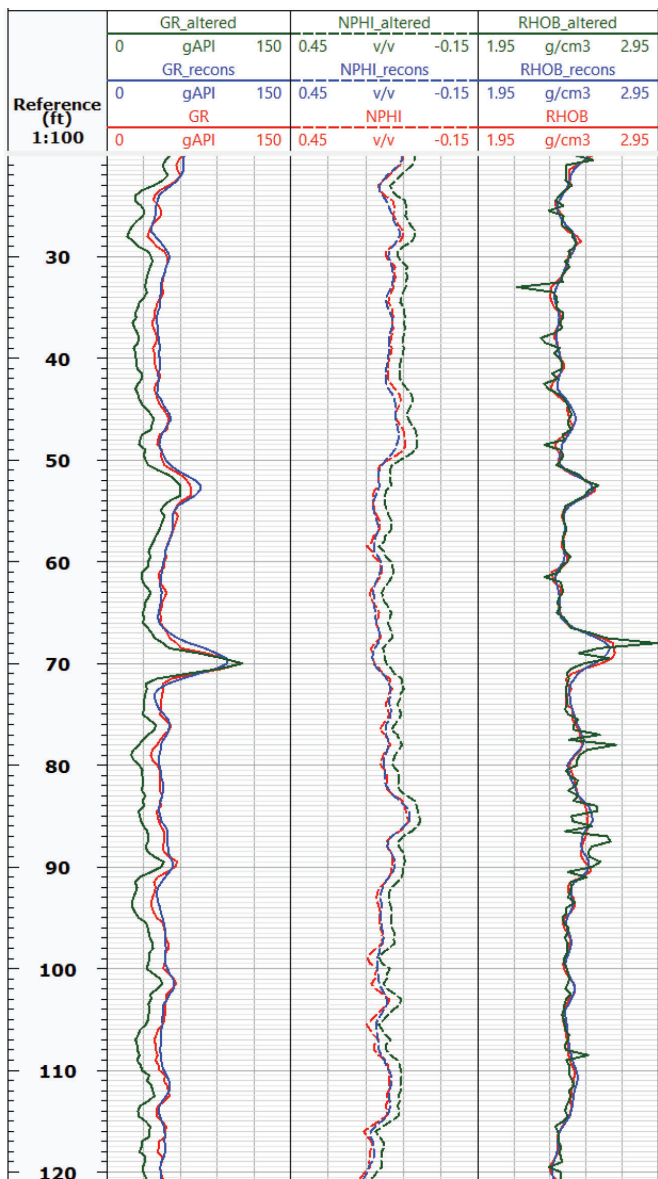


Fig. 13—Log plot depicting the ML log correction for a validation well with simultaneous alterations for gamma ray, neutron porosity, and density curves. The first track shows the measured depths. The second track shows the gamma ray (GR). The third track shows the neutron porosity (NPHI), and the fourth track contains the density logs. The original curves are in red, the altered data are in green, and the ML-corrected curves are in dark blue.

Table 7—PSNR from Validation Well Sample with Synthetic Alteration Before and After MALC

PSNR (dB)	Before MALC	After MALC
GR	21.1	31.59
NPHI	23.9	34.91
RHOB	26.2	36.06

Table 8—RMSE from Validation Well Sample with Synthetic Alteration Before and After MALC

RMSE	Before MALC	After MALC
GR (gAPI)	13.22	3.95
NPHI (v/v)	0.04	0.01
RHOB (g/cm ³)	0.05	0.02

Table 9—Reference Values Associated With Pure Halite and Anhydrite

	DTC (μs/ft)	RHOB (g/cm ³)	NPH (v/v)	GR (gAPI)
Halite	67.00	2.04	-0.03	0.00
Anhydrite	50.00	2.98	-0.02	5.00

For the intervals associated with halite presenting density and compressional slowness close to the pure mineral, one expects that the gamma ray and the neutron porosity logs will share a similar distribution. Figure 14 shows the GR histograms for a subset of wells with relatively high similarity in halite intervals (a) and anhydrite intervals (b). Values for density, neutron porosity, and compressional slowness for halite and anhydrite can be found in Schlumberger (2009).

In the original logs for this data set, there are wells with apparent shifts relative to the values expected for gamma ray and neutron porosity. By computing and comparing the dissimilarity, we could select a subset of the wells with high dissimilarity as test wells for evaluating the ML model performance in the presence of field noise.

Figure 15 contains the gamma ray distribution from the halite zones (a) and anhydrite (b) on the test wells. Compared to Fig. 14, there is more significant variability between the wells regarding the mode and distribution shape.

Some of the wells exhibit a high dissimilarity compared to the predominant trend, and we observe a similar difference for the neutron porosity.

The input logs used in the Groningen data set are density, neutron porosity, formation resistivity, and compressional slowness. To apply the model to other wells with a similar formation, in the Groningen data set, we used the following as input logs: original gamma ray, neutron porosity, density, compressional, and logarithmic of resistivity, and as output, we derived the corrected gamma ray and neutron porosity logs.

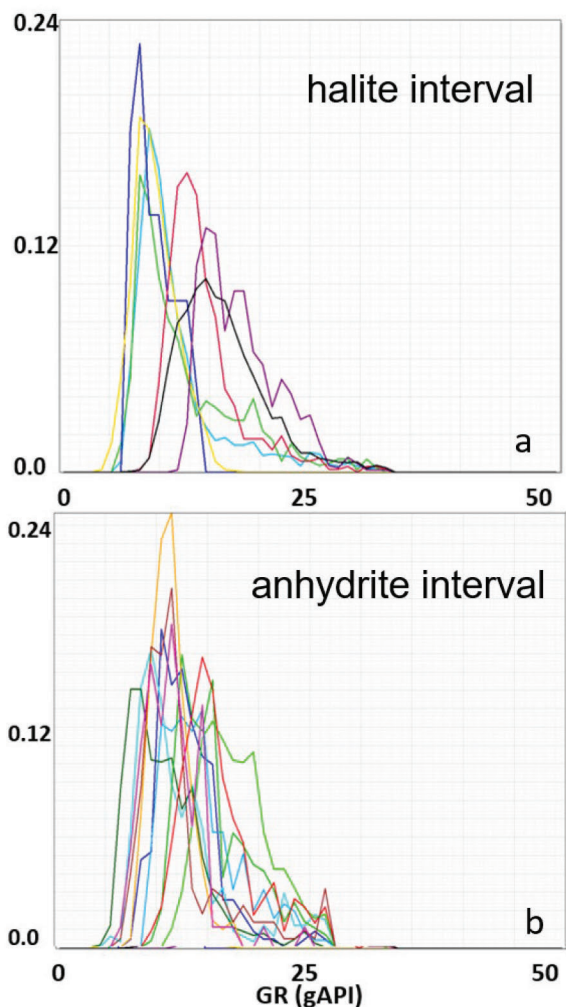


Fig. 14—Histogram with gamma ray log distribution for 10 wells with near-expected behavior over the halite interval (a) and anhydrite interval (b), with the x-axis between 0 and 50 gAPI.

We selected as test wells the ones with high dissimilarity on gamma ray or neutron porosity logs distribution for either anhydrite or halite layers and picked the remaining wells as training and validation wells.

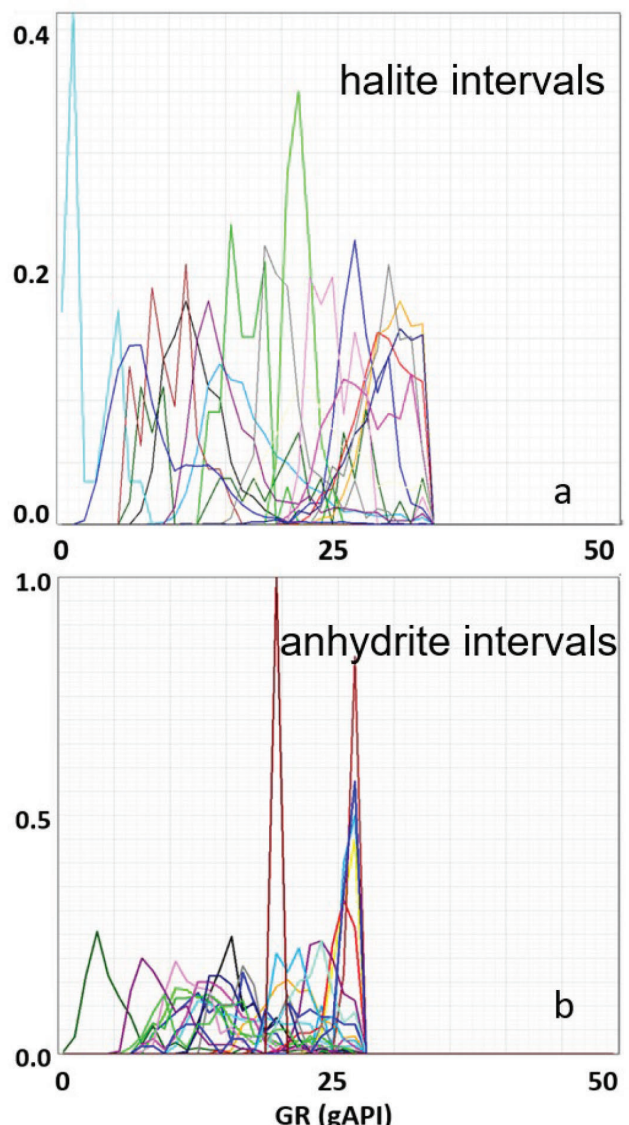


Fig. 15—Gamma ray distributions for the halite zones (a) and anhydrite intervals (b) in the Groningen Field test wells, presenting more variation than the training wells.

The theoretical solution or expert-edited curves are unavailable for the test wells in this case. Therefore, we resort to the ML-corrected log histograms and log plot visualizations to understand the behavior in a depth-by-depth analysis. Histograms in Fig. 16 contain the gamma ray distribution for the halite (a) and anhydrite (b) zones in the test wells after the ML correction, the same wells shown in Fig. 15a and Fig. 15b. The distributions in Fig. 15 have a more significant dissimilarity amidst the zones, and ML-corrected log distributions in Fig. 16 have a lower dissimilarity among the zones. These fixed log distributions are similar to the training wells presented in Fig. 14.

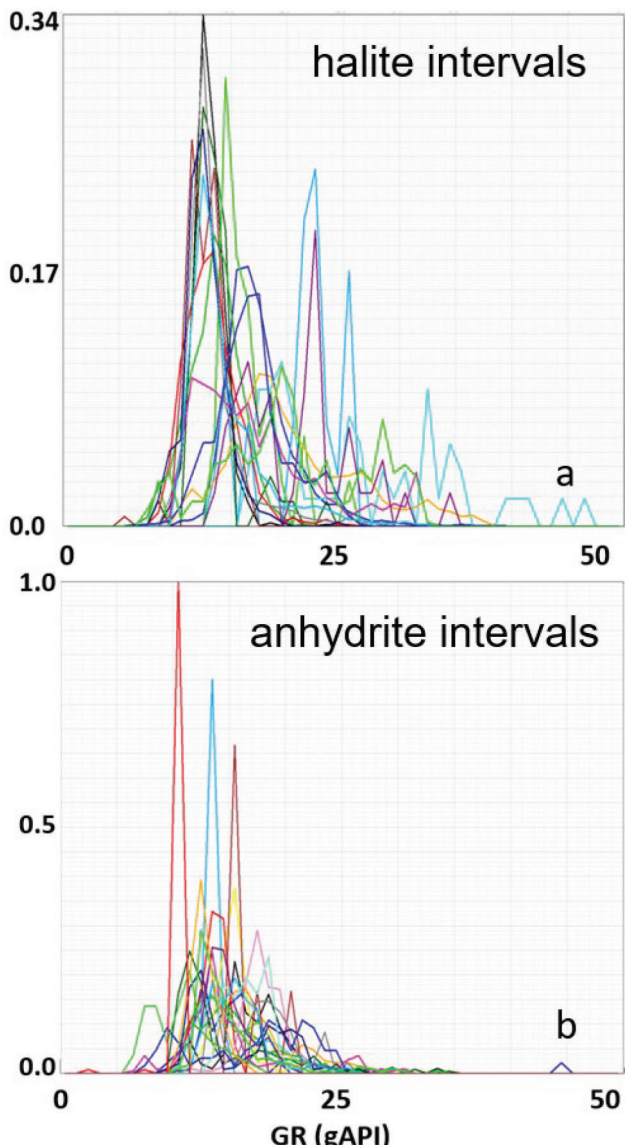


Fig. 16—Gamma ray distribution for halite zones (a) and anhydrite intervals (b) in the Groningen Field test wells after ML correction.

The log plots in Figs. 17 and 18 show the results in a depth-by-depth fashion for the MALC application in Test Well A. Track 3 contains the original (red) and corrected (blue) gamma ray logs. The statistical mode is 27 gAPI in zones with halite and 24 gAPI in zones with anhydrite before correction and 14 gAPI in both zones after correction. It is

also possible to notice that the correction is more intense in the top region and decreases with measured depth (MD). Track 4 shows that the original (red) and corrected (blue) neutron porosity logs are similar, and the model applies no apparent shift in that interval.

A second test case for applying the ML correction methodology is presented in Fig. 18. In this case, the model performed corrections to the gamma ray and neutron porosity simultaneously. For this well, the original neutron porosity in halite had a mode of 0.046 v/v, while after the correction, the mode reduced to -0.01 v/v, showing a similar behavior as in the training wells. It is important to notice an increase in borehole diameter in the presence of halite, which coincides with the increase in the ML-applied neutron porosity correction intensity.

The original gamma ray log had a mode of 7 gAPI in halite and 8 gAPI in anhydrite; after correction, the mode for gamma ray logs in both zones is 13 gAPI. In this case, it is important to remember that the model does not use information from reference values for halite and anhydrite or borehole diameter. Instead, it captures the expected behavior from the training wells and contextually applies the correction to increase their similarity.

After analyzing the ML-corrected logs for the reference zones, we can visualize the results in wells that showed a significant correction. One example can be seen in Test Well C in Fig. 21. Here, we notice a significant correction in the gamma ray log, which exhibits a consistently larger value than other wells in this field. This well has been identified as an outlier in our other ML applications, indicating an anomalous behavior compared to the other wells. The predicted gamma ray for this well using the remaining logs provided a consistently lower value than the original one, and the mismatch identified before was confirmed to be due to inconsistency in the log measurements for this well. The zones with unusually high gamma ray at the bottom of the reservoir were corrected to an expected range.

Tracks 2 and 3 in Fig. 19 contain the uncertainty band associated with the GR- and NPHI-corrected logs. This uncertainty band varies with depth and, in this well, increases near the bottom of the logged interval in zones with larger gamma ray values.

Deep Learning for Multiwell Automatic Log Correction

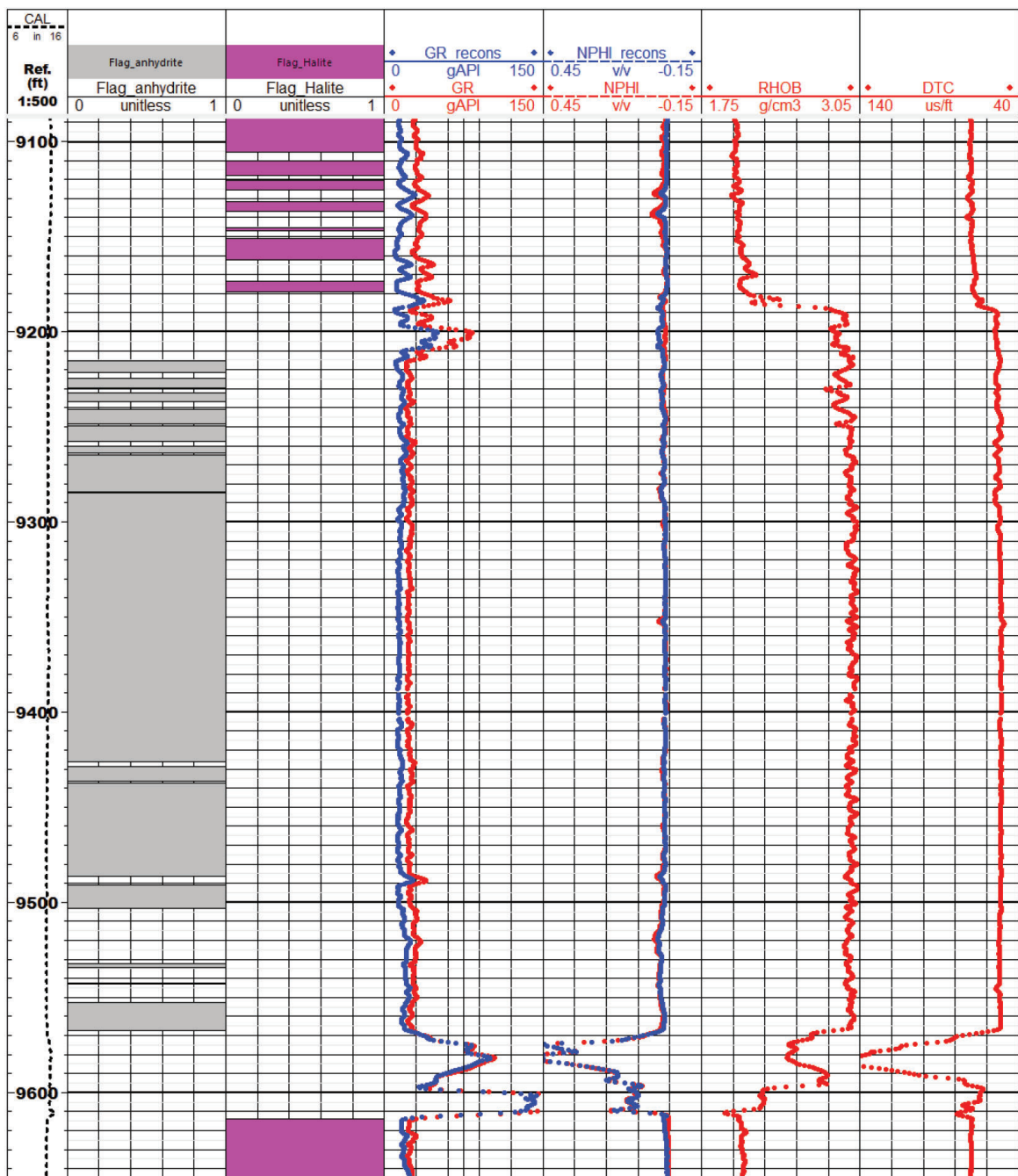


Fig. 17—Log plot showing the ML-corrected logs (blue) and original logs (red) for Test Well A in the Groningen Field. Track 2 contains an anhydrite flag. Track 3 includes the halite flag. Track 4 contains gamma ray logs. Track 5 contains neutron porosity logs. Track 6 contains the density log, and Track 7 has the compressional slowness log.

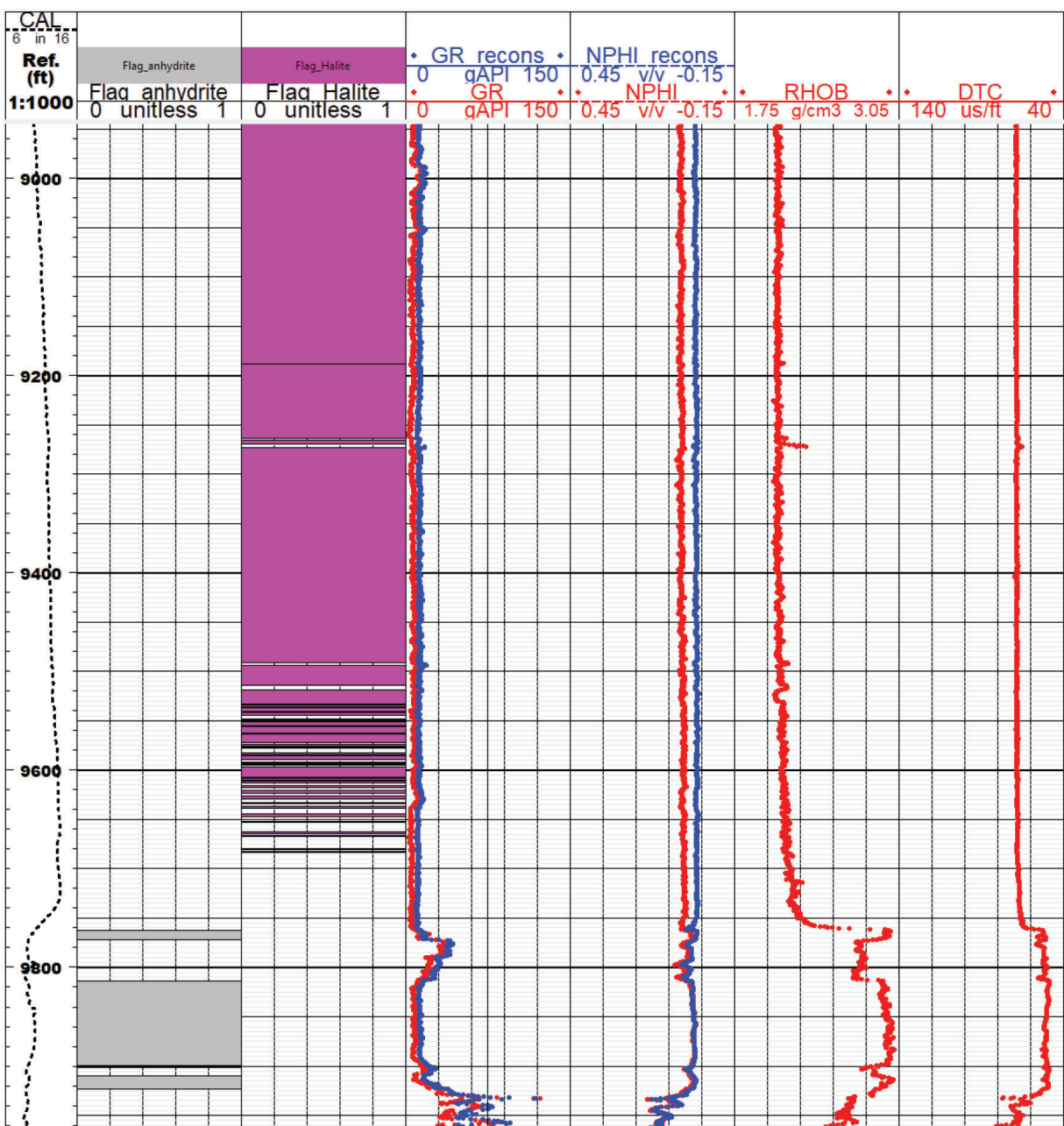


Fig. 18—Log plot showing the ML-corrected logs (blue) and original logs (red) for Test Well B in the Groningen Field. Track 2 contains the anhydrite flag. Track 3 has the halite flag. Track 4 contains gamma ray logs. Track 5 contains neutron porosity logs. Track 6 contains the density log, and Track 7 contains the compressional slowness log.

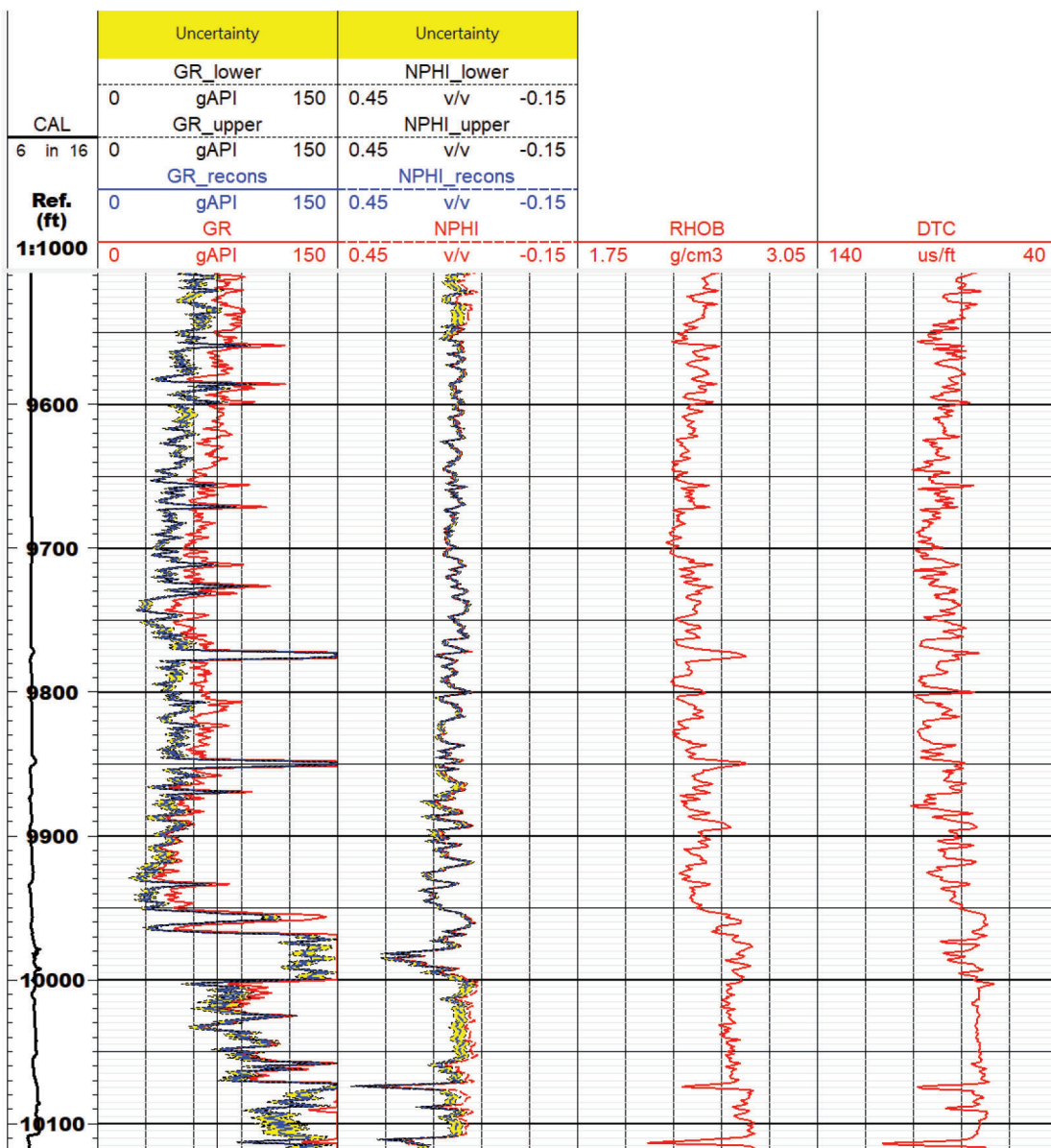


Fig. 19—Log plot showing the ML-corrected logs (blue) and original logs (red) in Training Well C. Track 1 contains caliper and measured depths. Track 2 has gamma ray logs. Track 3 contains neutron porosity logs. Track 4 contains the density log, and Track 5 contains the compressional slowness log.

The example in Fig. 20 shows the application of the ML method to a test well, including zones with halite and anhydrite, along with the main reservoir interval. It is possible to notice an almost constant shift in neutron porosity in the halite interval between 9,650 to 9,940 ft and the anhydrite intervals between 10,060 and 10,100 ft, indicating that the ML method learned the contextual nature over multiple formation types and provided a consistent result for the ML correction. It is also possible to notice a high uncertainty in the corrected gamma ray log. The correction indicates a shift

to a lower value than the logged data and shows a confidence interval for that correction.

To illustrate the effect of the ML correction in the dissimilarity matrix, we included three test wells with anhydrite zones (Well A, Well B, and Well D) and a typical training well and limited the GR distribution on the anhydrite layers. The result can be seen in Table 10 and Table 11.

The ML correction reduced the dissimilarity between any pair of test wells and the dissimilarity between the test wells and the training well.

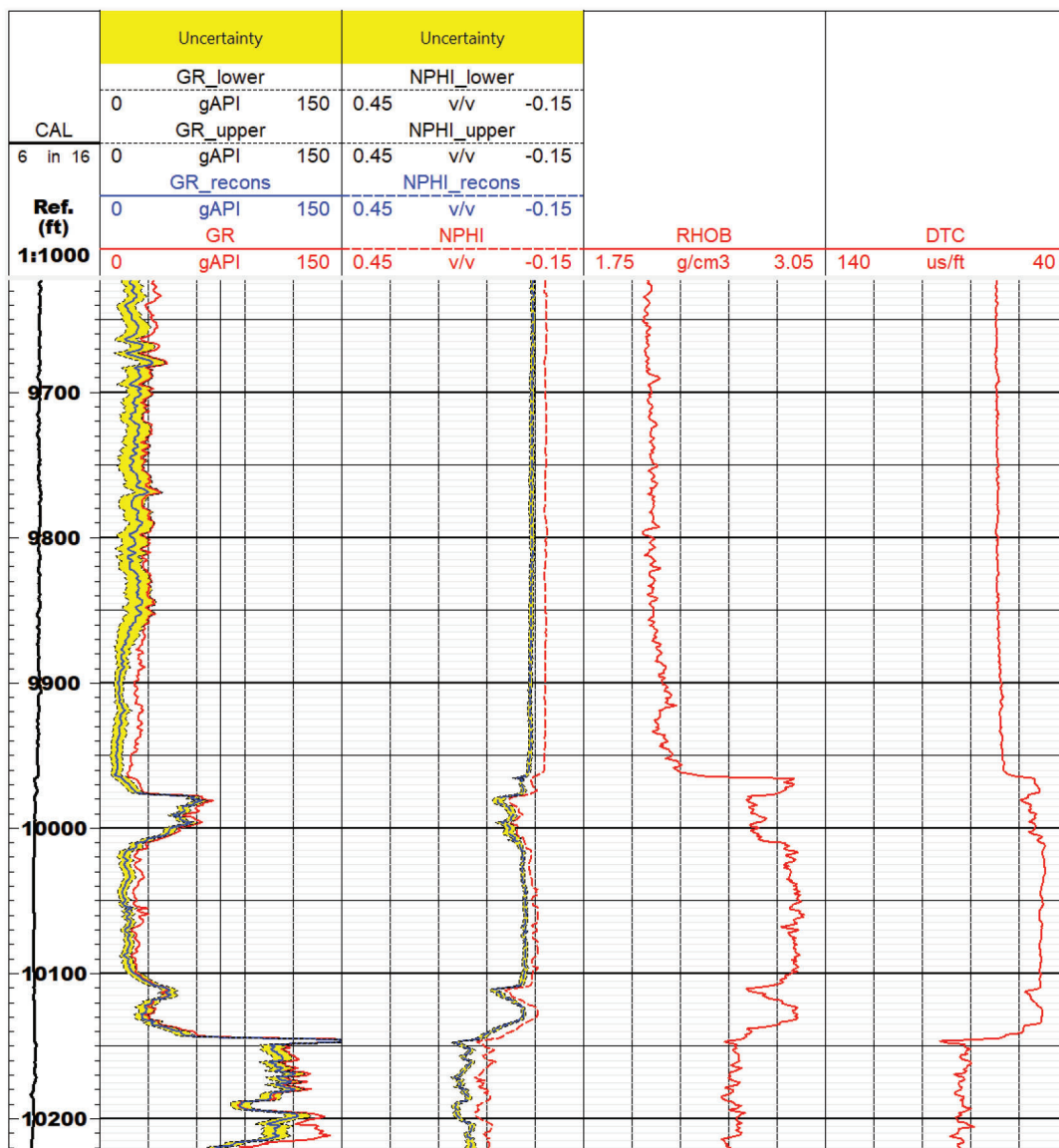


Fig. 20—Log plot showing the ML-corrected logs (blue) and original logs (red) in Training Well D. Track 1 contains caliper and measured depths. Track 2 contains gamma ray logs. Track 3 contains neutron porosity logs. Track 4 contains the density log, and Track 5 has the compressional slowness log.

Table 10—Dissimilarity Matrix for the Original Gamma Ray Logs Distribution for the Anhydrite Zones

	Well A	Well B	Well D	Training Well
Well A	0.00	0.74	0.32	0.60
Well B	0.74	0.00	0.71	0.63
Well D	0.32	0.71	0.00	0.50
Training Well	0.60	0.63	0.50	0.00

Table 11—Dissimilarity Matrix for ML-Corrected Gamma Ray Distribution for the Anhydrite Zones

	Well A	Well B	Well D	Training Well
Well A	0.00	0.20	0.30	0.31
Well B	0.20	0.00	0.36	0.30
Well D	0.30	0.36	0.00	0.30
Training Well	0.31	0.30	0.30	0.00

The histograms in Fig. 21 contain the gamma ray log distribution for the four wells in Tables 10 and 11 from the original logs and after applying MALC to the test wells, respectively. Both Table 10 and upper plot (Fig. 21a) indicate that Well B (in green) presents high dissimilarity compared to other wells, Wellbores A and D present low discrepancy between them, and the training well is dissimilar to all the three test wells. The ML-corrected gamma ray distribution for the three test wells plus the original gamma ray distribution for one training well contained in Table 11 are plotted in the histogram in Fig. 21b, which confirms MALC. All wells became less dissimilar in a pairwise analysis and closer to the training well used in this example.

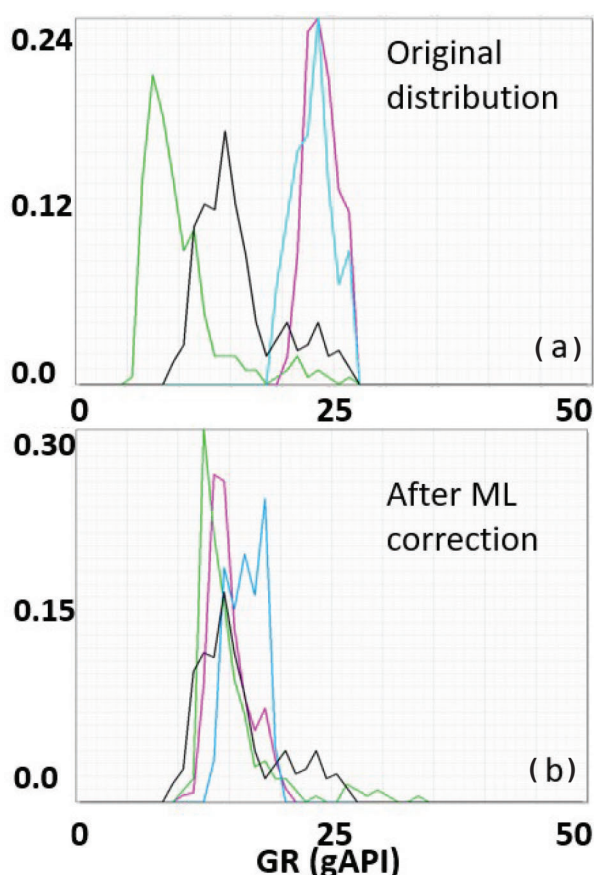


Fig. 21—Gamma ray distribution for three test wells and a training well from the Groningen data set in zones with mostly anhydrite. Well A is plotted in magenta, Well B in green, Well D in blue, and the training well in black. Upper plot (a) contains the original GR distribution, and lower plot (b) contains the gamma ray distribution after the ML correction.

CONCLUSIONS

This work presents MALC, an innovative way to perform log correction focusing on systematic errors that can affect the measurements due to miscalibration or borehole effects and random noises. The central proposition of this workflow is understanding the expected behavior for the logs based on samples extracted from training wellbores (type wells) and being able to correct logs from nearby wells that are in similar formation types. One assumption is that the training wells (type wells) can be used as reference wells to guide the correction applied during the inference stage.

The deep learning method comprises a 1DCNN with a multiscale architecture like U-Net. During training, controlled random and systematic errors are added to the input logs to replicate field occurrences, which teaches the ML model how to provide corrected outputs.

We presented successful applications to two data sets with different challenges. The Bakken data set contained 21 wells with high-quality gamma ray, density, neutron porosity, and resistivity logs. The ML method successfully corrected errors in test wells where we had added synthetic noise to the gamma ray only and both gamma ray and neutron porosity logs simultaneously. In both cases, the ML-corrected logs were similar to the original data, representing the formation properties.

The Groningen Field test presents inherent field alteration on gamma ray and neutron porosity. To separate wells to be used as test wells, we used a selection of wells with higher dissimilarity, focusing on halite and anhydrite zones since they could be easily identified. We use the remaining wells as training and validation data for building the ML model.

The results present good visual quality, and when reviewing the results for the reference halite and anhydrite zones, the distribution after the ML correction has an increased similarity with the training wells, with a mode and distribution shape like the values found in the training wells. We successfully applied this method to other data sets in different formations focusing on synthetic and field noise in the gamma ray and neutron porosity.

These cases show that the model works for both synthetic shifts and alterations in scaling factor, added to the data set, with varying intensity, and wells with original field noise, and we will continue testing in scenarios with expert-corrected logs for evaluating the model performance.

To create the current method, we estimated the expected alterations for each of the logs by reviewing the literature and analyzing field data from multiple data sets. We are working to improve the method with an increase in understanding of the distribution regarding the field noise presence.

The methodology includes using dissimilarity (D) and the Kullback-Leibler (KL) divergence to measure differences in the log distributions to identify groups of similar wells and outliers and evaluate the correction results. We also include a quantitative model performance evaluation using RMSE, Pearson correlation coefficient, and MAE to quantify the improvement when the ground truth is available for a well or interval that has not been seen during training.

An advantage of MALC compared to traditional methods is that our approach provides an answer that is consistent in some specific zones, such as anhydrite and halite, without explicitly giving this information directly to the model. The ML method can discover and maintain consistency without the need to manually identify those areas and referent values. This work presents the results on such layers for quality control of the results, but they do not represent an input to the ML model.

Another advantage of MALC is the self-supervised techniques based on denoising to train the deep learning model. This approach increases the range of potential applications to fields without expert-corrected logs, a common scenario when handling this problem.

Finally, the varying uncertainty can help an expert to select zones or intervals to perform quality control or include an uncertainty band in future interpretations.

ACKNOWLEDGMENTS

The authors thank SLB for providing the resources and opportunity to carry out this research project. Thanks to Lin Liang and Lalitha Venkataraman for their valuable feedback on the methodology in the first version of this work and for the reviewers that helped to improve the quality and completeness of this work.

The authors would like to thank Nederlandse Aardolie Maatschappij (NAM) and Utrecht University for providing the Groningen data set to the public under the Creative Commons Attribution 4.0 license.

Data associated with this research are available and can be obtained by contacting the corresponding author: vsimoes@slb.com.

The authors would like to acknowledge the use of TensorFlow, licensed under Apache License 2.0. TensorFlow

is an end-to-end open-source platform for machine learning. It has a comprehensive, flexible ecosystem of tools, libraries, and community resources that lets researchers push the state-of-the-art in ML and developers to easily build and deploy ML-powered applications.

NOMENCLATURE

Abbreviations

1D	= one dimensional
1DCNN	= unidimensional convolutional neural network
CAL	= caliper
CNN	= convolutional neural network
D	= dissimilarity
DTC	= compressional slowness
GR	= gamma ray
KL	= Kullback–Leibler
MAE	= mean absolute error
MAE_90	= mean absolute error disregarding the 10 percentiles with the largest error
MALC	= multiwell automatic log correction
ML	= machine learning
MSE	= mean square error
MSE_90	= mean square error disregarding the 10 percentiles with the largest error
NPHI	= neutron porosity
PSNR	= peak signal-to-noise ratio
Ref.	= reference or measured depth
RESD	= formation resistivity
RHOB	= density
RMSE	= root mean square error
RMSE_90	= root mean square error disregarding the 10 percentiles with the largest error
WAE	= window-based convolutional neural network autoencoder

REFERENCES

- Abubakar, A., Di, H., Kaul, A., Li, Z., Simoes, V., Truelove, L., and Zhao, T., 2022, Deep Learning for End-to-End Subsurface Modeling and Interpretation: An Example From the Groningen Gas Field, *The Leading Edge*, **41**(4), 259–267. DOI: 10.1190/tle41040259.1.
- Abubakar, A., Kulkarni, M., and Kaul, A., 2021, Automating Well Log Correlation Workflow Using Soft Attention Convolutional Neural Networks, Paper SPE-205985 presented at the SPE Annual Technical Conference and Exhibition, Dubai, UAE, 21–23 September. DOI: 10.2118/205985-MS.

- Aly, A.M., Hunt, E.R., Pursell, D.A., and McCain, W.D., Jr., 1997, Application of Multi-Well Normalization of Open Hole Logs in Integrated Reservoir Studies, Paper SPE-38263 presented at the SPE Western Regional Meeting, Long Beach, California, USA, 25–27 June. DOI: 10.2118/38263-MS.
- Anemangely, M., Ramezanzadeh, A., Amiri, H., and Hoseinpour, S.A., 2019, Machine Learning Technique for the Prediction of Shear Wave Velocity Using Petrophysical Logs, *Journal of Petroleum Science and Engineering*, **174**, 306–327. DOI: 10.1016/j.petrol.2018.11.032.
- Chen, G., Chen, L., and Li, Q., 2020a, Comparison and Application of Neural Networks in LWD Lithology Identification, *IOP Conference Series: Earth and Environmental Science*, 2nd International Conference on Advances in Civil Engineering, Energy Resources and Environmental Engineering, **526**(1), 012146, Nanning, China, 22–24 May. DOI: 10.1088/1755-1315/526/1/012146.
- Chen, W., Yang, L., Zha, B., Zhang, M., and Chen, Y., 2020b, Deep Learning Reservoir Porosity Prediction Based on Multilayer Long Short-Term Memory Network, *Geophysics*, **85**(4), WA213–WA225. DOI: 10.1190/geo2019-0261.1.
- de Jager, J., and Visser, C., 2017, Geology of the Groningen Field—An Overview, *Netherlands Journal of Geosciences*, **96**(5), S3–S15. DOI: 10.1017/njg.2017.22.
- Endres, D.M., and Schindelin, J.E., 2003, A New Metric for Probability Distributions, *IEEE Transactions on Information Theory*, **49**(7), 1858–1860. DOI: 10.1109/TIT.2003.813506.
- Gal, Y., and Ghahramani, Z., 2016, Dropout as a Bayesian Approximation: Representing Model Uncertainty in Deep Learning, *Proceedings of the 33rd International Conference on Machine Learning*, **48**, 1050–1059, New York, New York, USA, 19–24 June. URL: <http://proceedings.mlr.press/v48/gal16.pdf>. Accessed November 2, 2022.
- Gibbs, A.L., and Su, F.E., 2002, On Choosing and Bounding Probability Metrics, *International Statistical Review*, **70**(3), 419–435. DOI: 10.2307/1403865.
- Kingman, D.P., and Ba, J., 2015, Adam: A Method for Stochastic Optimization, 3rd International Conference for Learning Representations, San Diego, California, USA, 7–9 May. DOI: 10.48550/arXiv.1412.6980.
- Loshin, D., 2008, The Value of Data Quality, Chapter 5, in Loshin, D., editor, *Master Data Management*, first edition, 87–103, The MK/OMG Press. ISBN: 978-0123742254.
- McDonald, A., 2021, Data Quality Considerations for Petrophysical Machine Learning Models, *Petrophysics*, **62**(6), 585–613. DOI: 10.30632/PJV62N6-2021a1.
- Neinast, G.S., and Charles, C.K., 1973, Normalization of Well Log Data, Paper I, *Transactions, SPWLA 14th Annual Logging Symposium*, Lafayette, Louisiana, USA, 6–9 May.
- Quartero, E.M., Bechtel, D., Leier, A.L., and Bentley, L.R., 2014, Gamma-Ray Normalization of Shallow Well-Log Data With Applications to the Paleocene Paskapoo Formation, Alberta, *Canadian Journal of Earth Sciences*, **51**(5), 452–465. DOI: 10.1139/cjes-2013-0148.
- Ronneberger, O., Fischer, P., and Brox, T., 2015, U-Net: Convolutional Networks for Biomedical Image Segmentation, *Proceedings, Part III, Medical Image Computing and Computer-Assisted Intervention—MICCAI 2015*, Munich, Germany, 5–9 October, Lecture Notes in Computer Science, **9351**, Springer. DOI: 10.1007/978-3-319-24574-4_28.
- Schlumberger, 2009, *Log Interpretation Charts*, 279–280. URL: <https://www.slb.com/resource-library/book/log-interpretation-charts>. Accessed November 2, 2022.
- Shier, D.E., 2004, Well Log Normalization: Methods and Guidelines, *Petrophysics*, **45**(3), 268–280.
- Simoes, V., Maniar, H., Zhao, T., Abubakar, A., and Akkurt, R., 2022, A Comparative Study for Machine-Learning-Based Methods for Log Prediction, Paper 0067, *Transactions, SPWLA 63rd Annual Logging Symposium*, Stavanger, Norway, 11–15 June. DOI: 10.30632/SPWLA-2022-0067.
- Xu, C., Bayer, W.S., Wunderle, M., and Bansal, A., 2016, Normalizing Gamma-Ray Logs Acquired From a Mixture of Vertical and Horizontal Wells in the Haynesville Shale, *Petrophysics*, **57**(6), 638–643.

APPENDIX 1 – RISKS OF NOT INCLUDING ZONATION INFORMATION AND REFERENCE LITHOLOGIES WHEN PERFORMING LOG NORMALIZATION USING TRADITIONAL APPROACHES

One advantage of the proposed method vs. traditional approaches is that we don't need to identify reference lithologies, while conventional normalizations require the identification of some reference (type) wells and in all wells to be corrected. If one doesn't use zonation information, the final correction using fixed log values' percentiles might be biased even on simple geologies, as presented in Fig. A1.1.

Using a hypothetical case similar to that presented in Fig. A1.1, we exemplify the risks of using a traditional methodology without identifying the lithology. We can consider a simplified subsurface containing two primary lithologies associated with gamma ray around 30 gAPI (with yellow dots) and gamma ray around 70 gAPI (black dashes).

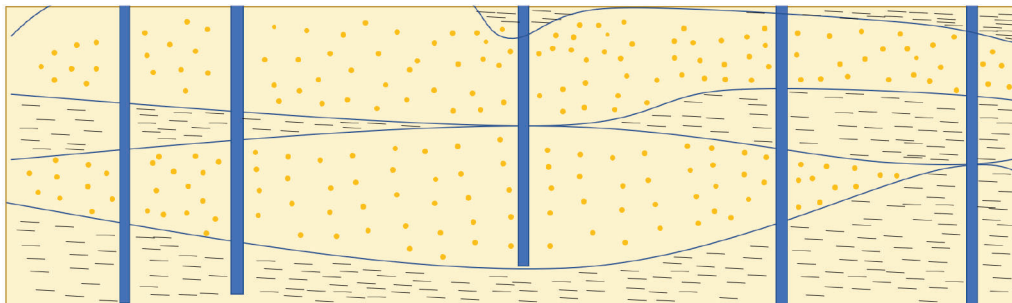


Fig. A1.1—Scheme for a simplified formation with two lithologies represented with yellow dots and black dashes associated with a gamma ray distribution with an average of 30 gAPI and 70 gAPI and five logged wells crossing the formation.

Assuming a normal distribution for the gamma ray logs around the values 30 gAPI and 70 gAPI and weighted average according to the volume of each formation type, we get the distributions for five wells crossing those layers as in Fig. A1.2 (top histogram). Even without evidence of misalignment between those gamma ray logs, the differences in the proportion of Lithology 1 and 2 cause the 10th and 90th percentiles of the gamma ray distributions to present variation among the wells, as indicated by the misalignment in the black and blue crosses in Fig. A1.2 (top histogram).

One can attempt to use a linear transformation (see Shier, 2004; Quartero et al., 2014), as in Eq. A1.1 to align the 10th and 90th percentiles according to the 10th and 90th percentiles for the type well presented in red.

$$GR_{norm} = \left(\frac{x_{ref,90} - x_{ref,10}}{P_{90} - P_{10}} \right) (GR_{orig} - P_{10}) + x_{ref,10} \quad (\text{A1.1})$$

In Eq. A1.1, GR_{norm} represents the normalized gamma ray, GR_{orig} represents the original gamma ray log, $x_{ref,10}$ and $x_{ref,90}$ represent the 10th and 90th percentiles for the reference or type well (plotted in red in the example presented in histograms in Fig. A1.2), and P_{10} and P_{90} represent the 10th and 90th percentiles of the original gamma ray log wellbore GR log being normalized.

The histogram for the percentiles-based normalized GR distribution is presented in Fig. A1.2 (bottom histogram), where one can see the local maximums misalignment. Those peaks are associated with the averages of the two lithologies, indicating that percentile normalization provides a poor correction even in that simplified scenario because it did not consider the weights associated with each of the intervals logged by each well.

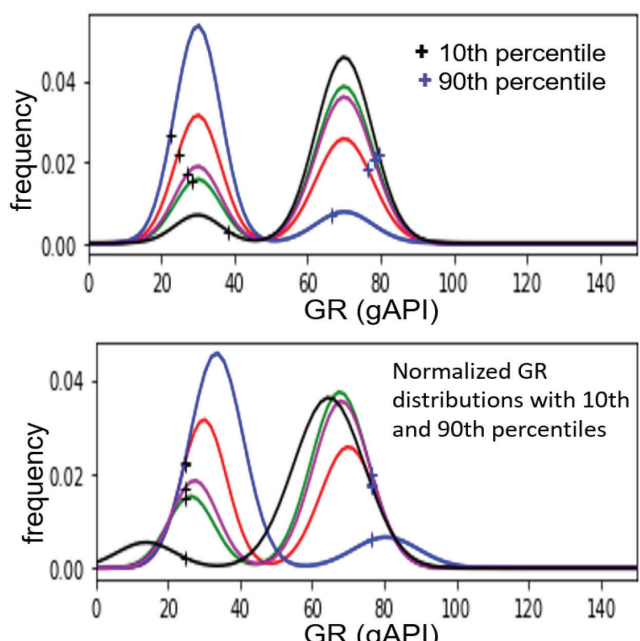


Fig. A1.2—Top histogram contains the original gamma ray distribution for five wells crossing two different lithologies as simplified in Fig. A1.1, as well as the 10th and 90th percentiles for each well in black and blue crosses, respectively. The bottom histogram contains the same distributions after performing a fixed linear transformation to align the 10th and 90th percentiles using the curve distribution in red as reference (well type).

In contrast to this fixed linear methodology, the proposed MALC solution doesn't assume equal proportions of different lithologies across the well because we do a local correction using multiple wellbore-log types for getting contextual information. The ML method also has information from neutron porosity, resistivity, and compressional slowness, and it can automatically identify the expected formation properties and apply the necessary corrections to

improve the wellbore-log consistency. The information of multiple logs also represents an advantage in the presence of laminated formations with a scale smaller than the vertical tool resolution.

ABOUT THE AUTHORS



Vanessa Simoes is currently a data scientist on the Digital Subsurface Intelligence team at SLB, Houston. She graduated in computing and applied mathematics (2006) from the University of Sao Paulo (USP). She received her MSc degree in mathematical modeling (2009) and her PhD degree in mathematics (2013) from the Instituto de Matemática Pura e Aplicada (IMPA). She concluded two specialization programs in data analytics and deep learning at Pontifical Catholic University (PUC), Rio de Janeiro (2018). Vanessa joined SLB in 2013 and has worked in Rio de Janeiro, Boston, and Houston. She is currently working on log quality control projects using machine learning to enhance subsurface data quality. Her technical interests include acoustics, data analysis, statistics, and rock physics.



Hiren Maniar is a global ML/AI scientist with SLB actively developing ML methods for subsurface interpretation purposes. His interdisciplinary experiences encompass data analysis, machine learning, mathematical analysis, numerical modeling, inverse problems, and signal processing, and he has developed data-driven applications ranging from neuroscience to geosciences and from banking/retail to cancer. He earned his PhD degree in wave hydrodynamics from the Massachusetts Institute of Technology (MIT).



Aria Abubakar is currently the head of Data Science for Digital Subsurface Solutions. His main responsibility is to oversee and coordinate the utilization of artificial intelligence, machine learning, and data-analytics technology for subsurface applications throughout SLB. He received an MSc degree in electrical engineering (1997) and a PhD degree in technical sciences (2000), both from the Delft University of Technology,

Netherlands. He joined Schlumberger-Doll Research in Ridgefield, Connecticut, USA (2003), where he remained for 10 years, ending his tenure as a scientific advisor and manager of the Multi-Physics Modeling and Inversion Program. From 2013 until mid-2017, he was the interpretation engineering manager at SLB Houston Formation Evaluation in Sugar Land, Texas. From mid-2017 until mid-2020, he was the data analytics program manager for Software Technology and then started in his current position. Aria is quite active in SEG and currently serves as an associate editor of *Geophysics*, member of the Research Committee, director of SEAM, and 2021 SEG Annual Meeting Technical Program Co-Chair. Aria was a 2014 SEG North America Honorary Lecturer and a 2020 SEG-AAPG Distinguished Lecturer. He holds 40 US patents/patent applications, has published five book/book chapters, and has written more than 90 scientific articles in journals, 200 conference proceedings papers, and 60 conference abstracts. He also has presented more than 300 invited and contributed talks at international conferences, institutes, and universities.



Tao Zhao is the data science manager for interpretation at SLB. Tao joined SLB in 2019 as a senior data scientist, developing deep learning applications in seismic imaging. Before his tenure at SLB, Tao was a research geophysicist at Geophysical Insights, where he advanced research on deep learning methods applied to seismic interpretation. Tao received PhD and MS degrees in geophysics from the University of Oklahoma and the University of Tulsa and a BE degree in exploration geophysics from the China University of Petroleum (East China).